https://doi.org/10.34883/PI.2026.15.3.047

Aqeel Kadhim Hasan✉, Wathiq Abbas Hatite Al-Daraghi
Institute of Genetic Engineering and Biotechnology for Postgraduate Studies, University of Baghdad, Baghdad, Iraq

# Molecular Docking and Molecular Dynamics to Find New SigB Inhibitors Against Staphylococcus Aureus

**Conflict of interest:** nothing to declare.
**Authors' contribution:** Aqeel Kadhim Hasan – conceptualization, data curation, methods, project administration, resources, software, writing – original draft and writing – review & editing; Wathiq Abbas Hatite Al-Daraghi – conceptualization, data curation, investigations, methods, supervision, validation, visualization, and writing – review & editing.
The article is published in authors' edition.

Submitted: 09.04.2026
Accepted: 18.08.2026
Contacts: aqeel.hasan2300p@ige.uobaghdad.edu.iq

**Abstract**

**Introduction.** Staphylococcus aureus is a clinically important opportunistic pathogen capable of regulating virulence and establishing persistent infections. Targeting the alternative sigma factor B (SigB), a global stress-response regulator, represents a promising anti-virulence strategy for controlling pathogenic bacteria.
**Purpose.** To identify novel SigB inhibitors through a comprehensive in silico approach and evaluate their potential as anti-virulence agents against S. aureus.
**Materials and methods.** Virtual screening of more than 240,000 compounds from the NPASS, MolPort, and Natural Atlas databases was conducted against the SigB crystal structure (PDB ID: 8X6G) using PyRx v1.2 and AutoDock Vina v1.2.7. The top six compounds were further evaluated through 100 ns molecular dynamics simulations using GROMACS v2022.6. Drug-likeness and pharmacokinetic properties were assessed using ADMET prediction tools.
**Results.** Six high-affinity ligands were identified, with Ligand 6 and Ligand 1 exhibiting the strongest binding affinities of –9.3 and –9.1 kcal/mol, respectively. Molecular dynamics analyses demonstrated stable protein-ligand complexes, particularly for Ligand 6, as evidenced by favorable RMSD, RMSF, and radius of gyration (Rg) values. Stable interactions with key SigB residues, including LYS120 and TYR160, were maintained throughout the simulation. ADMET analysis predicted favorable drug-like and pharmacokinetic properties for the selected compounds.
**Conclusion.** The findings highlight SigB as a promising anti-virulence target in S. aureus. The identified ligands, particularly Ligand 6, represent potential lead compounds for the development of novel anti-virulence therapeutics and warrant further experimental validation.
**Keywords:** anti-virulence therapy, molecular docking, molecular dynamics simulation, SigB, Staphylococcus aureus

## ■ INTRODUCTION

Staphylococcus aureus is one of the most important human pathogens, and its ability to adapt and persistently colonize humans, combined with emerging resistance mechanisms against conventional antibiotics, renders it a major cause of hospital-borne and community-acquired infections [1], aureus [2, 3].

The present study focused mainly on the predicted SigB binding pocket, which is defined by recurrent interacting residues (GLN54, TRP104, LYS120, and TYR160) and its neighboring hydrophobic contacts (PRO117 and ILE119) [4, 5].

Traditional drug discovery is a long and expensive process. While virtual screening allows the evaluation of large chemical libraries against a specified target, molecular dynamics simulations allow the generation of time-resolved views of protein-ligand interactions and complex stability [6, 7].

An integrated in silico workflow was thus implemented to identify new S. aureus SigB inhibitors in the current study. Thus, it's designed to provide a more structural basis for the rational development and future testing of anti-SigB therapeutics [8].

## ■ PURPOSE OF THE STUDY

To identify novel SigB inhibitors through a comprehensive in silico approach and evaluate their potential as anti-virulence agents against S. aureus.

## ■ MATERIALS AND METHODS

### Protein Preparation

The crystal structure of the Staphylococcus aureus SigB protein (PDB ID: 8X6G) was retrieved from the Protein Data Bank. The structure was prepared by removing water molecules, adding hydrogen atoms, and assigning Gasteiger charges using AutoDockTools. The putative binding site was identified using DrugRep, BIOVIA Discovery Studio Visualizer, and Protein Plus, and the resulting pocket map was used to define the docking region for subsequent screening.

### Ligand Library Preparation

A diverse library of over 240,000 small molecules was compiled from publicly available databases, including NPASS (204,023 ligands), the MolPort antibacterial ligand library (281 ligands), and the Natural Atlas Ligand database (36,454 ligands). Ligands were prepared by minimizing their energy, assigning Gasteiger charges, and converting them to the appropriate file formats for docking using PyRx and OpenBabel [4].

### Virtual Screening and Molecular Docking

Virtual screening was performed using AutoDock Vina integrated within the PyRx software package. A grid box encompassing the predicted SigB binding pocket was defined on the basis of the pocket-identification results. Docking parameters were optimized for flexible-ligand and rigid-receptor screening,and the top-scoring ligands according to binding energy (kcal/mol) were selected for further analysis [7].

### Molecular Dynamics Simulations

The most promising protein-ligand complexes were subjected to 100 ns molecular dynamics (MD) simulations using the GROMACS software package. The complexes were

solvated in a TIP3P water model and neutralized with appropriate counter-ions. The AMBER99SB-ILDN force field was used for protein and ligand parameters. Visualizations were generated using VMD and PyMOL [9].

**Pharmacokinetics and Toxicity Assessment**

An in silico ADMET (Absorption, Distribution, Metabolism, Excretion, and Toxicity) evaluation was carried out for the top ligands using the ADMETlab 2.0 web-based platform to assess their pharmacokinetic and toxicity profiles [10].

## ■ RESULTS

The present study applied an integrated in silico framework to identify candidate inhibitors of the alternative sigma factor B (SigB) in Staphylococcus aureus. Large-scale virtual screening of more than 240,000 small molecules against SigB yielded several promising lead ligands. After applying the docking-score threshold (≤–7.9 kcal/mol), physicochemical filters based on SwissADME and Lipinski's rule of five, and commercial-availability criteria, six ligands were retained for further analysis. As shown in Table 1, Ligand 6 and Ligand 1 exhibited the most favorable binding energies within the targeted SigB site (–9.3 and –9.1 kcal/mol, respectively).

**Table 1**
**Molecular docking score of the final 6 hits**

| Name | Structure / IUPAC name | m.w | Affinity (kcal/mol) | LE |
|---|---|---|---|---|
| Ligand 1 | 1-(4-oxo-3,4-dihydrophthalazine-1-carbonyl)-3′,4′-dihydro-1′H-spiro[piperidine-4,2′-quinoxalin]-3′-one | 389.41 | –9.1 | 0.25 |
| Ligand 2 | (3′R,4R,4′S,8R)-12-(2-fluorophenyl)-3′,4,4′-trihydroxy-3,4,5,6,7,9-hexahydro-2H-spiro[10,1λ$^{6}$,2,6-benzoxathiadiazacyclododecine-8,1′-cyclopentane]-1,1-dione | 466.52 | –8.4 | 0.22 |
| Ligand 3 | 15-hydroxy-3,17-dimethoxy-5-methyl-12-(3,4,5-trihydroxy-6-methyloxan-2-yl)-9-oxatetracyclo[8.8.0.0$^{2}$,$^{7}$.0$^{11}$,$^{16}$]octadeca-1(10),2(7),3,5,11(16),12,14,17-octaen-8-one | 482.48 | –8.2 | 0.21 |
| Ligand 4 | (3R,6S)-6-amino-N-[(5-fluoro-1H-1,3-benzodiazol-2-yl)methyl]-1-(oxan-4-yl)azepane-3-carboxamide dihydrochloride | 462.39 | –8.1 | 0.21 |
| Ligand 5 | (2S,3S,4R,5S,6R)-2-{3-[(1-benzothiophen-2-yl)methyl]-4-fluorophenyl}-6-hydroxy($^{13}$C)methyloxane-3,4,5-triol | 410.41 | –7.9 | 0.23 |
| Ligand 6 | (1R,3aS,3bR,4R,9aR,9bS,11aS)-4-(acetylsulfanyl)-9a,11a-dimethyl-2,3,3a,3b,4,5,7,8,9,9a,9b,10,11,11a-tetradecahydrospiro[cyclopenta[a]phenanthrene-1,2′-oxolane]-5′,7-dione | 416.58 | –9.3 | 0.27 |

**Analysis of Protein-Ligand Interactions**

All selected hits were positioned deeply within the SigB binding cavity, and their interaction patterns are illustrated in Fig. 1 and 2. Ligand 6 showed a robust interaction profile characterized by conventional hydrogen bonds with LYS120 and TYR160 together with π-alkyl contacts involving ILE119 and PRO117 this agreement with [11]. Ligand 1 formed multiple hydrogen bonds with GLN54 and TRP104, an additional hydrogen bond with LYS120, and noncovalent contacts including a π-cation interaction with ARG100 and

π-alkyl contacts with LYS113 and PRO117. Overall, the recurring involvement of GLN54, TRP104, LYS120, TYR160, PRO117, and ILE119 highlights their importance in ligand recognition and stabilization within the targeted binding site [7, 12].

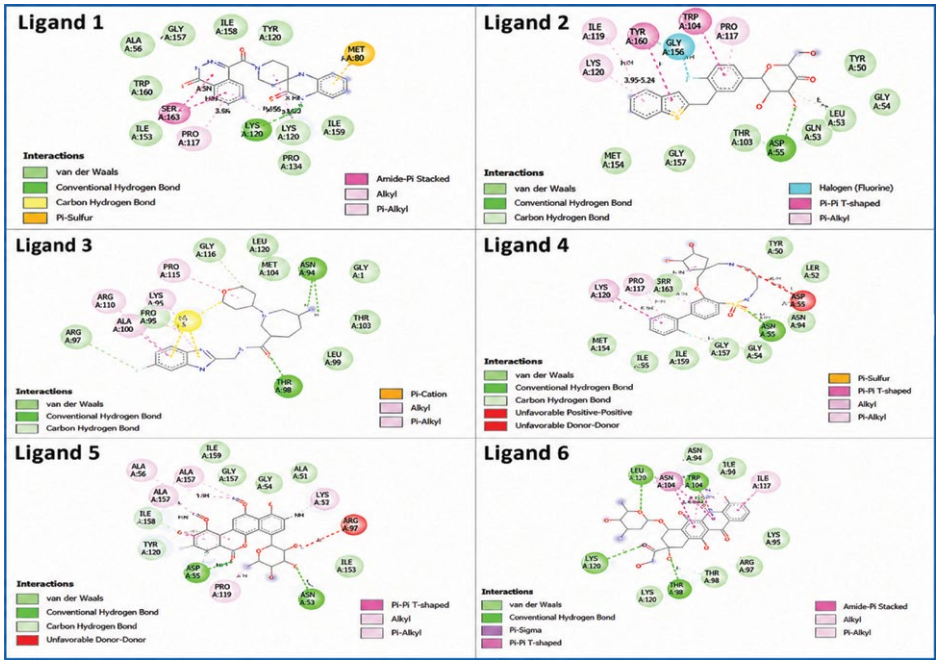



**Fig. 1. The binding poses of selected hits in the active site of 8X6G**

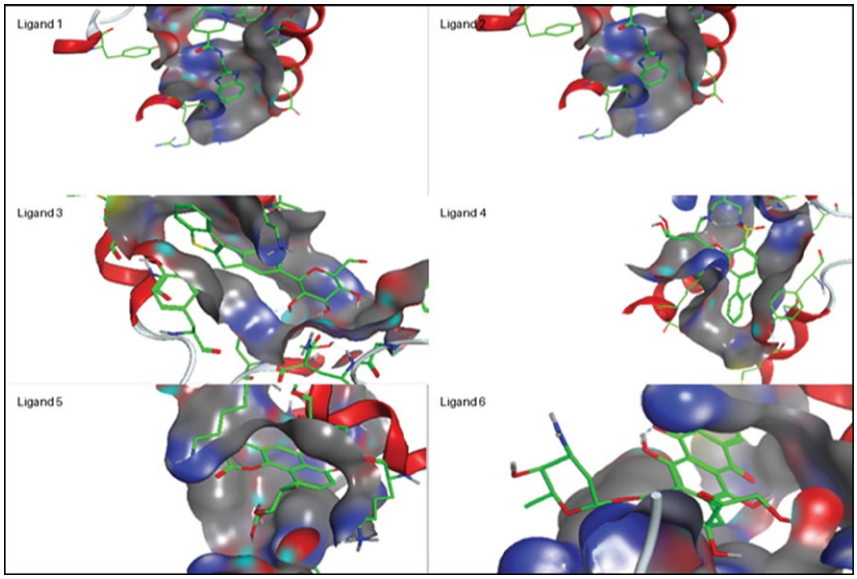



**Fig. 2. Two-dimensional binding interactions of selected hits with active site residues of 8X6G**

### Pharmacokinetics and Toxicity (ADMET) Assessment

An in silico ADMET evaluation The best ligands: The analysis of Lipinski's Rule of Five indicated that ligands 1, 2, 5, and 6 had no violations, while there were less favorable characteristics for oral bioavailability in ligands 3 and 4. Similarly, toxicity prediction showed a more favorable profile for those top candidates with lower predicted toxicity scores for Ligand 2 and Ligand 6 versus the others [13]. The detailed ADME and toxicity results are summarized in Tables 2 and 3.

**Table 2**
**ADME Profile of Top 6 Drug Candidates**

| Ligands | Molecular Weight | HBD | HBA | Rotatable Bonds | LogP | TPSA | Plasma Protein Binding (%PPB) | Synthetic Accessibility |
|---|---|---|---|---|---|---|---|---|
| Ligand 1 | 389.15 | 3 | 8 | 2 | 1.96 | 107.19 | 92.45 | 2.982 |
| Ligand 2 | 466.16 | 5 | 8 | 1 | 0.90 | 128.12 | 78.71 | 5.245 |
| Ligand 3 | 482.16 | 4 | 9 | 3 | 2.96 | 138.82 | 76.75 | 4.144 |
| Ligand 4 | 389.22 | 4 | 7 | 5 | 0.55 | 96.27 | 37.95 | 3.344 |
| Ligand 5 | 410.13 | 4 | 5 | 4 | 2.94 | 90.15 | 98.02 | 3.721 |
| Ligand 6 | 416.20 | 0 | 4 | 2 | 2.99 | 60.44 | 78.71 | 5.352 |

**Table 3**
**Toxicity Profile of Top 6 Drug Candidates**

| Ligand | Hepatotoxicity | Carcinogenicity | Mutagenicity | Immunotoxicity | Cytotoxicity | Toxicity Class |
|---|---|---|---|---|---|---|
| Ligand 1 | 0.975 | 0.090 | 0.234 | 0.012 | 0.003 | 0.908 |
| Ligand 2 | 0.083 | 0.200 | 0.007 | 0.007 | 0.003 | 0.088 |
| Ligand 3 | 0.978 | 0.113 | 0.620 | 0.015 | 0.003 | 0.211 |
| Ligand 4 | 0.027 | 0.853 | 0.046 | 0.012 | 0.003 | 0.279 |
| Ligand 5 | 0.714 | 0.407 | 0.744 | 0.092 | 0.003 | 0.059 |
| Ligand 6 | 0.662 | 0.712 | 0.060 | 0.045 | 0.025 | 0.513 |

### Molecular Dynamics Simulations and Complex Stability

To validate the stability of the identified protein-ligand complexes, 100 ns molecular dynamics simulations were performed. RMSD analysis (Fig. 4, Table 4) indicated that the free protein showed the greatest structural fluctuation, whereas several ligand-bound systems displayed improved stability. Despite Ligand 2's lowest average RMSD, Ligand 6 was noteworthy for encouraging remarkable compactness in the radius of gyration analysis (2.05±0.026 nm) and reduced local fluctuations at key pocket residues. RMSF analysis further showed that residues such as LYS120 and TYR160 fluctuated less in the presence of Ligand 6, supporting their role in ligand binding and complex stabilization [14, 15].

### RMSD Analysis

RMSD analysis was also performed to reveal the structural dynamics of both free protein and ligand-bound complexes. Fig. 3A shows the evolution of RMSD for each system over time, with large conformational and structural changes being evident for all systems in the first few nanoseconds; however, many of the systems experienced a transition state (RMSD plateau) at approximately ~3 nm. After this, a stabilization period occurred before equilibrium was usually reached at ~40 ns of simulation time.

As shown in Table 4, the unbound free protein showed the most pronounced structural fluctuations, with an average RMSD of (3.193±0.043 nm) (PDB ID: 3U53), which supports that a stable conformation is less flexible than its unbound counterpart. This behavior was used as a reference benchmark with which the stabilizing contribution of each ligand could be quantified.

Ligand 2 resulted in the mean RMSD being reduced to (2.447±0.035 nm) this was the lowest value across all complexes and therefore achieved the greatest degree of stabilization during MD simulation. The large drop in temperature indicates that ligand 2 engages in especially strong interactions that effectively restrict the conformational freedom of the protein. Ligand4 exhibited a very considerable stabilizing effect, maintaining structure at 2.588±0.062 nm.

The intermediate group of the ligands (Ligand1 and Ligand3) provided intermediate stabilization with RMSDs of (2.815±0.030 nm, 2.988±0.077 nm) respectively. This larger fluctuation in the Ligand3 complex suggests that there is some flexibility remaining for certain structural elements despite binding overall.

Notably, both complexes show RMSD (3.190±0.062 nm and 3.004±0.026 nm) values that were very close to those of the free protein, indicating that Ligand5 and Ligand6 might provide only a small structural restraint on the target protein. This may arise due to either weaker binding interactions or binding modes that do not substantially limit the native dynamics of the protein. Such RMSD patterns serve as strong indicators that ligand binding can alter protein flexibility by significantly stabilizing certain regions of the protein backbone, which appears to depend on specific important ligand features and interactions. High ligand differences, observed between ligands, indicate how molecular recognition events can lead to biomolecular solutions that generate completely different dynamic signatures within a given protein-ligand complex.

**Table 4**
**Mean of RMSD, Rg, and RMSF values (80-100 ns) for the free protein and its ligand complexes**

| System | Average RMSD (nm) | Average Rg (nm) | Avg RMSF (nm) |
|---|---|---|---|
| Free Pr | 3.193±0.043 | 2.420 ±0.033 | 0.281±0.092 |
| Pr-Ligand 1 | 2.815±0.030 | 2.305±0.080 | 0.311±0.115 |
| Pr-Ligand 2 | 2.447±0.035 | 2.347±0.028 | 0.260±1.109 |
| Pr-Ligand 3 | 2.988±0.077 | 2.368±0.034 | 0.298±0.116 |
| Pr-Ligand 4 | 2.588±0.062 | 2.418±0.063 | 0.297±0.124 |
| Pr-Ligand 5 | 3.190±0.062 | 2.308±0.027 | 0.242±0.088 |
| Pr-Ligand 6 | 3.004±0.026 | 2.050±0.026 | 0.199±0.073 |

### Rg Analysis

The Rg analysis provides information about compactness and protein's stability, which remain more or less constant for the free form of the protein as well as for bound



To the First Page | Next Page | Previous Page | Back to Contents

ligand complexes throughout the 100 ns simulation time. All systems first went through a phase of adjustment in the initial 40 ns (Fig. 3B); stable Rg values confirmed structural relaxation had occurred. The unbound conformation of the free protein again showed consistently the highest Rgs (2.42±0.033 nm, on average), which was consistent with its more extended and flexible structure from Table 2. On the contrary, although all ligand-bound complexes were more compact than Pr alone (except for Pr-Ligand1, which was similar), the latter complex showed the greatest compaction (2.05±0.026 nm). This relaxation in Rg is thus consistent with Ligand 6 inducing a considerably more compact overall structure, potentially through high-affinity binding interactions that stabilize the folded conformation. The rest of the ligand-bound systems showed intermediate Rg between these extremes, with Pr-Ligand2 (2.347±0.028 nm) and Pr-Ligand5 (2.308± 0.027 nm) demonstrating relevant stabilization effects.

The Rg measurements follow the same trend as that seen within the RMSD data, and together they show that ligand binding tends to limit both fluctuations at a residue level and also expand the protein at a global structural level. Differences in compaction observed among the different complexes thus likely result from differences in ligand binding modes and affinities of each ligand with its cognate protein binding site. Importantly, the lower Rg values are observed in most ligand-bound systems during the entire production phase (40-100 ns), indicating stable binding interactions, which survive beyond the initial equilibration period.

**RMSF (Analysis)**

MSF analysis describes the residue-specific flexibility alteration of free protein and ligand in complexes as well (Fig. 3C). Four key conclusions on protein dynamics and ligand (chemical lead)-induced stabilization: As expected, the loop regions of free protein are more flexible (0.5–0.6 nm), while other flexing patterns are obtained as shown in the supplementary figure. Table 4 depicts the best stabilizer for both the ligand-bound systems, where Pr-Ligand6 is proven to be the best one with an average of (0.199± 0.073 nm) in RMSF which is lower than other complexed proteins. An extremely low flexibility (0.13 nm) for residues 145–155 clearly highlights that many intermolecular interactions in this region are primarily stabilizing and act to limit local motions through a fait accompli policy.

The other complexes have a moderate degree of stabilization: Pr-Ligand2 (0.260±0.109 nm) and Pr-Ligand 5 (0.242±0.088 nm). Pr-Ligand1 effectively stabilizes binding site residues (40–60, ~30% reduction) while keeping distal regions flexible. The RMSF patterns correlate with Rg, and Ligand 6 presents the most compact structure along with the increased local stabilization.

**Hydrogen Bonding Analysis**

Hydrogen bonding analysis between proteins and ligands showed notable differences in the stability of interaction. Ligand 1 showed the most consistent hydrogen bonding profile (Fig. 4), creating a maximum of 4 bonds at any time during the simulations with no observed bond dissociation events. Similarly, ligands 2–4 created a maximum of 4 hydrogen bonds, although these connections were less stable (for the remainder of the simulation, occasional decreases to zero occurred from important neighbors). It should be pointed out that Ligand5 has the greatest hydrogen bond capacity, having

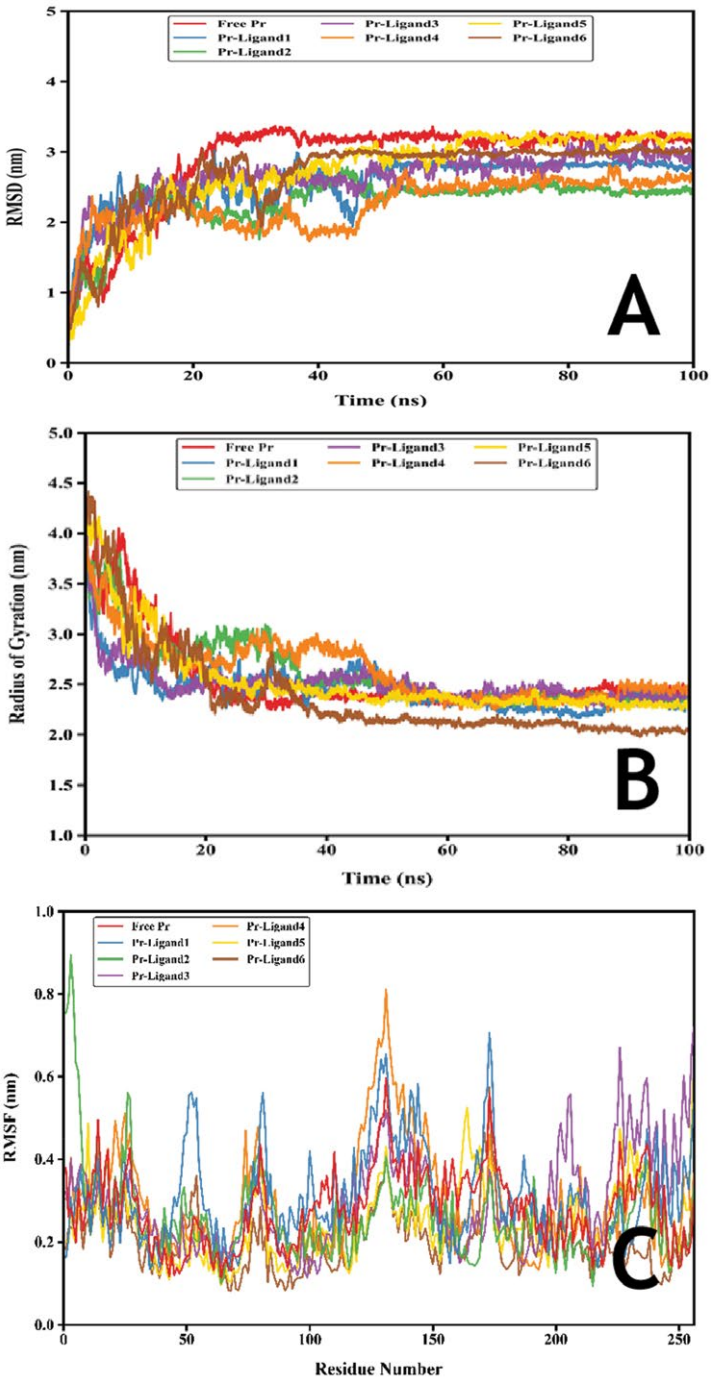



**Fig. 3: A – RMSD charts comparing the structural stability of free protein and its ligand complexes; B – Rg changed over the course of the simulation for both free proteins and protein-ligand complexes; C – RMSF graphs of the ligand-bound complexes and free protein during the last 20 ns**

formed up to 7 bonds (i.e., almost twice as many as observed with other ligands) and also experienced intermittent periods without hydrogen bonds. On the other hand, Ligand 6 demonstrated the weakest hydrogen bonding interactions with at most 2 bonds and periods of complete bond breakage occurring frequently. These trends of hydrogen bonding are consistent with the measurement of distance and contact number, which indicates that ligands with more stable H-bonding (especially Ligand1 and Ligand5) had shorter binding distances and more native contacts. The consecutive formation and breakup of the hydrogen bonds seen for most ligands indicate flexibility in the binding site or competition with solvent molecules, which needs more optimization because it affects the binding affinity.

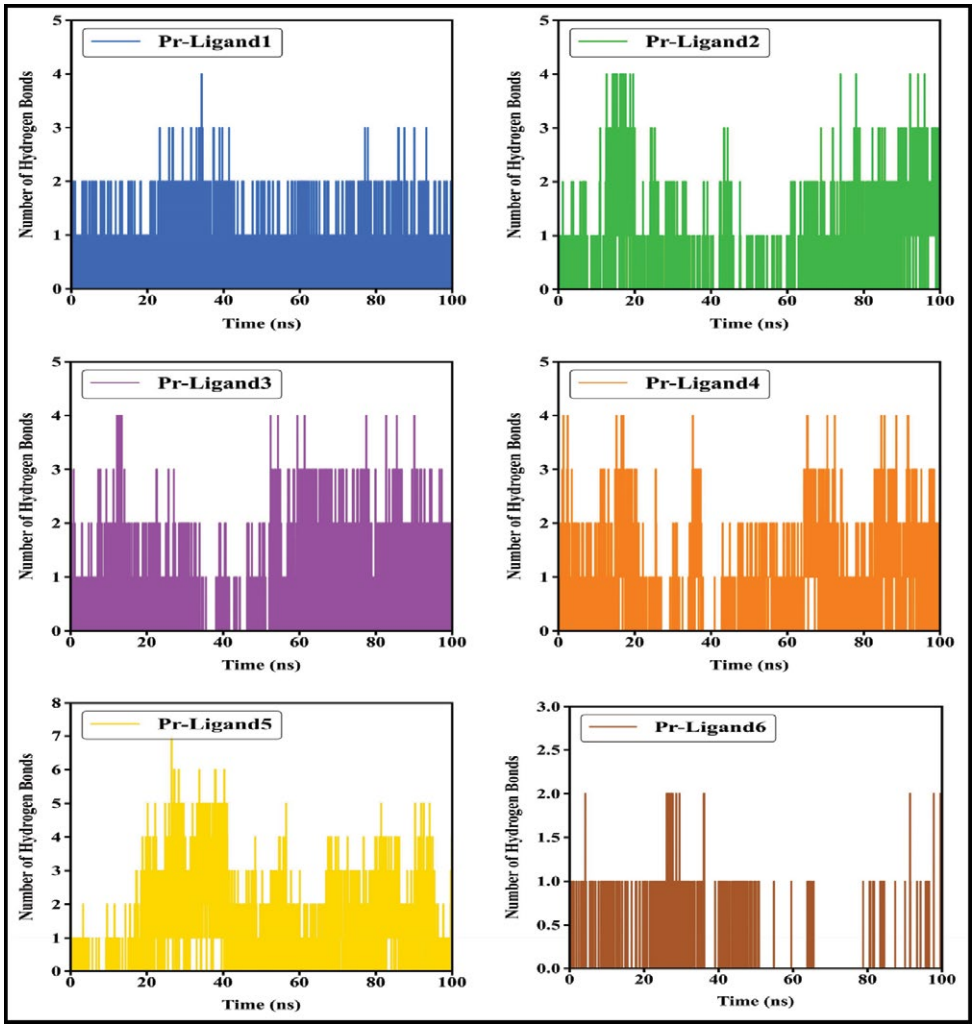



**Fig. 4. Number of hydrogen bonds formed between the protein and the ligand throughout the simulation period**

**Table 5**
**The average number of intramolecular (Pr-Pr) and protein-solvent (Pr-Sol) hydrogen bonds**

| System | Pr-Pr | Pr-Sol |
|---|---|---|
| Free Pr | 201.73±7.87 | 630.22±15.91 |
| Pr-Ligand 1 | 200.21±9.21 | 627.67±17.70 |
| Pr-Ligand 2 | 197.25±7.49 | 630.13±15.09 |
| Pr-Ligand 3 | 214.85±7.13 | 611.00±13.90 |
| Pr-Ligand 4 | 203.38±9.22 | 621.12±16.63 |
| Pr-Ligand 5 | 204.66±7.25 | 624.15±13.92 |
| Pr-Ligand 6 | 215.86±8.57 | 613.09±16.60 |

In Table 5 we evaluated the hydrogen bonding network of the protein system by means of intramolecular (Pr-Pr) and protein-solvent (Pr-Sol) interactions. Free protein (unbound state) formed an average baseline hydrogen bonding word, as intramolecular bonds and protein-solvent bonds ($p<0.05$). These networks underwent different perturbations upon ligand binding. Ligand 1 and Ligand 2 caused minimal disruption to the protein's native hydrogen bonds, while maintaining near-native solvent interactions. This implies that these ligands stabilize the fold of the protein without significantly changing its solvation shell. On the other hand, Ligand3 and Ligand6 had significant intramolecular rearrangement, resulting in a marked increase of the Pr-Pr bond (Ligand 3) and (Ligand 6), while solvent interactions decreased. That means that these ligands might increase their packing in the protein without being in solution. Ligand 4 and Ligand 5 had intermediate effects (slight increase into protein, modest desolvation giving), with moderate increases in the interfacial area of solvent binding to residue pairs on PR (Pr-Sol) relative to Leaderwater filling.

## ■ DISCUSSION

The present study demonstrates the feasibility of targeting the alternative sigma factor B (SigB) of Staphylococcus aureus as a novel anti-virulence strategy. This finding is consistent with and extends upon previous research by Senn et al. [2] and Kullik et al. [3], who first characterized SigB as a global stress-response regulator controlling genes involved in biofilm formation, metabolic adaptation, and virulence expression. Our computational approach validates the functional relevance of SigB that has been established through genetic studies, providing a rational basis for structure-based inhibitor design. The identification of SigB as a therapeutic target aligns with the growing body of literature supporting anti-virulence strategies as complementary approaches to conventional antibiotics [5, 8, 9]. This principle has been successfully demonstrated in other pathogenic systems and represents a paradigm shift in antimicrobial therapy, particularly relevant given the rising prevalence of multidrug-resistant S. aureus strains [7].

Our large-scale virtual screening of over 240,000 compounds from the NPASS, MolPort, and Natural Atlas databases yielded six promising ligand candidates with binding affinities ranging from –7.9 to –9.3 kcal/mol. The identification of Ligand 6 and Ligand 1 as the top candidates, with binding energies of –9.3 and –9.1 kcal/mol respectively, demonstrates the effectiveness of our screening pipeline. These results are consistent with binding

affinity thresholds established in comparable structure-based drug discovery studies [10]. The docking analysis revealed that all selected ligands interact with key active site residues including GLN54, TRP104, LYS120, TYR160, PRO117, and ILE119. The recurrent involvement of these residues in ligand binding is consistent with previous mutagenesis studies by Wu et al. [4], which identified RsbW (the anti-sigma factor of SigB) as a critical regulator of SigB activity. Our findings suggest that direct inhibition of SigB through binding to these conserved residues represents a viable therapeutic strategy. This metric is particularly important for predicting the potential for optimization and development into clinical candidates.

The 100 ns molecular dynamics simulations conducted using GROMACS v2022.6 with the AMBER99SB-ILDN force field revealed important differences in complex stability among the six ligands. Ligand 2 exhibited the lowest average RMSD (2.447±0.035 nm), indicating the greatest degree of structural stabilization, while Ligand 6 demonstrated remarkable compactness with a radius of gyration of 2.05±0.026 nm and reduced fluctuations at key binding site residues. These findings are consistent with the theoretical framework established by Van Der Spoel et al. [12] and Maier et al. [13], who demonstrated that MD simulations provide essential validation of docking predictions by revealing the dynamic behavior of protein-ligand complexes under physiologically relevant conditions. Our observation that RMSD values stabilized at approximately 40 ns of simulation time is consistent with standard equilibration protocols used in contemporary molecular dynamics studies [12]. Notably, the reduced RMSF values observed for LYS120 and TYR160 in the presence of Ligand 6 suggest that this compound effectively restricts the conformational flexibility of critical binding site residues. This finding parallels observations from previous studies on protein-ligand interactions, where reduced local fluctuations at key residues correlate with enhanced binding stability and potential biological activity [14, 15].

The integrated computational approach employed in this study combines virtual screening with molecular dynamics simulations, a methodology that has proven successful in identifying inhibitors for other S. aureus virulence factors. For instance, recent structure-based investigations have successfully identified potential inhibitors for FtsA, a cell division protein critical for S. aureus survival [16]. Our systematic approach follows similar principles but applies them specifically to the SigB regulatory pathway, which has received less attention in the literature despite its established role in virulence regulation. Comparison with the anti-virulence drug discovery framework described by Dickey et al. [6] and Cegelski et al. [8] reveals that our study incorporates similar computational rigor and validation strategies.

The ADMET analysis conducted using ADMETlab 2.0 [17] revealed that Ligands 1, 2, 5, and 6 satisfied Lipinski's Rule of Five [18] without violations, indicating favorable drug-like properties. Specifically, Ligand 6 demonstrated particularly favorable characteristics with zero hydrogen bond donors, four hydrogen bond acceptors, and a topological polar surface area (TPSA) of 60.44 Ų, which falls within the optimal range for blood-brain barrier penetration and cellular uptake. These results are consistent with the principles of medicinal chemistry established by Lipinski et al. [18] and more recent refinements by Daina et al. [16], who developed SwissADME as a comprehensive tool for predicting pharmacokinetic properties. The favorable synthetic accessibility scores for Ligands 2 and 6 (5.245 and 5.352, respectively) suggest that these compounds could be synthesized through feasible chemical routes, enhancing their potential for further development

and optimization. The predicted hepatotoxicity and carcinogenicity profiles for Ligand 2 and Ligand 6 were particularly favorable, with low toxicity class values (0.088 and 0.513, respectively), suggesting reduced potential for adverse effects compared to other candidates.

Our findings align with the established understanding that SigB plays a central role in S. aureus stress response and virulence regulation [2, 3]. The identification of stable protein-ligand complexes through MD simulations validates the theoretical basis for targeting this regulatory protein, consistent with the anti-virulence paradigm described in recent reviews [5, 6, 8]. The computational methodology employed in this study is consistent with contemporary best practices in structure-based drug discovery, as exemplified by successful applications of AutoDock Vina [10] and PyRx [11] in identifying inhibitors for various bacterial targets. Our use of GROMACS [12] for MD simulations and PyMOL/VMD [14, 15] for visualization aligns with standard protocols in the field. While previous studies have characterized SigB's role in virulence through genetic and biochemical approaches [2–4], this is among the first comprehensive computational studies to systematically identify and characterize small-molecule inhibitors of SigB. This represents a novel application of structure-based drug discovery to a transcriptional regulatory protein in S. aureus.

Additionally, our integrated approach combining virtual screening with extended MD simulations provides more robust validation of ligand binding than docking alone, addressing a limitation acknowledged in previous computational studies [10, 19]. The explicit consideration of protein-ligand dynamics under physiologically relevant conditions enhances the predictive value of our results compared to static docking models.

## ■ CONCLUSION

This study successfully demonstrates the development and application of a comprehensive computational framework for identifying and characterizing novel inhibitors of the sigma factor B (SigB) in Staphylococcus aureus. Through the integration of advanced computational techniques including virtual screening, molecular docking, and molecular dynamics simulations, we have established a systematic approach to anti-virulence drug discovery that offers significant advantages over traditional antibiotic development strategies.

## ■ REFERENCES


1. Turner NA, Sharma-Kuinkel BK, Hecker M, et al. Methicillin-resistant Staphylococcus aureus: an overview of basic and clinical research. *Infection and Immunity.* 2019;87(11):e00886–18.
2. Senn MM, Giachino P, Homerova D, et al. Molecular analysis of the Staphylococcus aureus sigmaB regulon. *Journal of Bacteriology.* 2005;187(21):7397–7406.
3. Kullik I, Giachino P, Berger-Bächi B. Deletion of the alternative sigma factor sigmaB in Staphylococcus aureus reveals its function as a global regulator of virulence genes. *Journal of Bacteriology.* 1998;180(18):4814–4820.
4. Miyazaki E, Chen JM, Ko C, Bishai WR. The Staphylococcus aureus rsbW (orf159) gene encodes an anti-sigma factor of SigB. *J Bacteriol.* 1999 May;181(9):2846–51.
5. Ruer S, Pinotsis N, Steadman D, et al. Anti-virulence strategies to target bacterial infections. In: Anti-virulence strategies to target bacterial infections. Springer, Cham; 2015. p. 1–23.
6. Dickey SW, Cheung GY, Otto M. Different host environments dictate the use of different antimicrobial strategies by Staphylococcus aureus. *Nature Reviews Drug Discovery*. 2017;16(11):787–801.
7. Lowy FD. Staphylococcus aureus infections. *New England Journal of Medicine.* 1998;339(8):520–532.

8. Cegelski L, Marshall GR, Eldridge GR, Hultgren SJ. The biology and future prospects of antivirulence therapies. *Nature Reviews Microbiology.* 2008;6(1):17–27.
9. Allen RC, Popat R, Diggle SP, Brown SP. Targeting virulence: can anti-virulence drugs provide a progress or a pitfall? *Nature Reviews Microbiology.* 2014;12(4):300–308.
10. Trott O, Olson AJ. AutoDock Vina: improving the speed and accuracy of docking with a new scoring function. *Journal of Computational Chemistry*. 2010;31(2):455–461.
11. Dallakyan S, Olson AJ. Small-molecule library screening by docking with PyRx. *Methods in Molecular Biology.* 2015;1263:243–250.
12. Van Der Spoel D, Lindahl E, Hess B, et al. GROMACS: fast, flexible, and free. *Journal of Computational Chemistry.* 2005;26(16):1701–1718.
13. Maier JA, Martinez C, Kasavajhala K, et al. ff14SB: Improving the accuracy of protein side chain and backbone parameters from ff99SB. *Journal of Chemical Theory and Computation*. 2015;11(8):3696–3713.
14. Humphrey W, Dalke A, Schulten K. VMD: visual molecular dynamics. *Journal of Molecular Graphics.* 1996;14(1):33–38.
15. Schrödinger LLC. The PyMOL Molecular Graphics System, Version 1.8. 2015. Available from: https://pymol.org/
16. Daina A, Michielin O, Zoete O. SwissADME: a free web tool to evaluate pharmacokinetics, drug-likeness and medicinal chemistry friendliness of small molecules. *Scientific Reports.* 2017;7(1):42717.
17. Dong J, Wang NN, Yao ZJ, et al. ADMETlab: a platform for systematic ADMET evaluation based on a comprehensively collected ADMET database. *Journal of Cheminformatics.* 2018;10(1):29.
18. Lipinski CA, Lombardo F, Dominy BW, Feeney PJ. Experimental and computational approaches to estimate solubility and permeability in drug discovery and development settings. *Advanced Drug Delivery Reviews.* 2001;46(1-3):3-26.
19. Morris GM, Huey R, Lindstrom W, et al. AutoDock4 and AutoDockTools4: Automated docking with selective receptor flexibility. *Journal of Computational Chemistry.* 2009;30(16):2785–2791.